

LETTER

A 100-M/s 2.6-pJ/pulse compact UWB impulse transmitter based on antenna-and-pulse-generator codesign

Hongming Lyu^{1a)}, Xiangyu Liu¹, and Aydin Babakhani¹

Abstract This work presents a novel concept of antenna-and-pulse-generator codesign for realizing FCC-regulation-compliant IR-UWB transmitters. The method contributes to a compact design that significantly reduces the overall device footprint and energy consumption. A Gaussian mono-pulse generator and a folded-dipole antenna with a bandwidth of 7.8–9.5 GHz are co-optimized, eliminating any matching sections. The energy consumption for each impulse emission is only 2.6 pJ and 100 Mpulse/s operation of the transmitter complies with the FCC mask. The transmitter of this kind shows promise for size-restricted and ultra-low power applications such as medical implants.

Keywords: UWB, impulse radio, ultra-low-power telemetry, medical implant

Classification: Microwave and millimeter-wave devices, circuits, and modules

1. Introduction

The unlicensed 3.1–10.6 GHz ultra-wideband impulse (IR-UWB) radio has remarkable advantages such as compact size, low power consumption, and circuitry simplicity. Because of these merits, it is especially popular for realizing low-power telemetries for numerous wearable and implantable applications [1, 2, 3, 4, 5, 6, 7, 8, 9, 10, 11, 12, 13].

Edge-combining is a widely used method in generating IR-UWB pulses [3, 5, 14, 15, 16, 17]. It has a simple circuit structure and removes the otherwise power-hungry local oscillators. To satisfy the Federal Communications Commission (FCC) emission limit, two methods have been primarily used to eliminate the low-frequency (<3.1 GHz) portion of radiation. First, multiple pulses with different delays are combined to create a short period of toggles with the center frequency amid 3.1–10.6 GHz, i.e., pulse-combining [14, 16]. This method, however, is at the expense of higher power consumption. Second, a pulse-shaping filter is added following a Gaussian mono-pulse generator, i.e., filtered edge-combining [5, 15, 17]. The filter can be implemented with either extra passive components or an active differentiator [15].

This letter proposes a new idea of directly utilizing the Tx antenna bandwidth to confine the spectrum of the radiated power. This method eliminates any pulse-shaping filters and reduces the power consumption. To implement

the idea, a Gaussian mono-pulse generator is designed to maximize the power transfer efficiency to a folded-dipole antenna with the input impedance of 300 Ω and the bandwidth of 7.8–9.5 GHz. The folded-dipole antenna has a fixed real input impedance at the resonant frequency, a relatively wide bandwidth, and a compact size. As a result, each impulse emission only consumes 2.6 pJ DC energy. Operation of the transmitter at a pulse rate of 100 M/s is demonstrated to comply with the FCC mask.

2. Circuit design

The circuit schematic of the transmitter is shown in Fig. 1. Each transition of the input signal triggers a Gaussian mono-pulse on either Out₁ and Out₂ nodes, which subsequently drives a folded-dipole antenna. While either output node emits a pulse, the other node is tied to GND. The receiver is based on energy detection scheme, and, therefore, does not differentiate Out₁-driven or Out₂-driven impulses. The folded-dipole antenna is selected for its compact size, wide bandwidth, and omnidirectional radiation pattern [18, 19, 20, 21, 22, 23], which is particularly promising for a wide range of efforts on the miniaturization of various medical implants [24, 25, 26, 27, 28, 29]. The input impedance of a folded-dipole antenna at the resonant frequency approximately equals 300 Ω [18].

Therefore, the gate-sizing of the Gaussian mono-pulse generator is designed to maximize the power transfer efficiency to 300 Ω load resistance as shown in Fig. 2(a). The close symmetry between Out₁ and Out₂ nodes is guaranteed. Circuit simulations across all process corners, i.e., typical-typical (TT), fast-fast (FF), slow-slow (SS), fast-slow (FS), and slow-fast (SF), verify that both the DC energy consumption and the delivered impulse energy are stable (Fig. 2(b)). In TT process corner, for instance, Out₁-driven and Out₂-driven pulses consume 2.75 pJ and 2.55 pJ DC energy, respectively.

The normalized fast Fourier transform (FFT) of the Out₁-driven and Out₂-driven pulses in different process corners are simulated as shown in Fig. 3(a) and (b), respectively. To accommodate the most process variation, the antenna bandwidth should cover 8–9 GHz.

3. Antenna design

The planar geometry of the folded-dipole antenna in this design is shown in Fig. 4. The bond wires have been taken into consideration.

¹Dept. of Electrical and Computer Engineering, University of California Los Angeles, Los Angeles, CA 90095, US

a) hongminglyu@ucla.edu

DOI: 10.1587/elex.16.20190672

Received November 6, 2019

Accepted November 11, 2019

Publicized December 2, 2019

Copiedited December 25, 2019

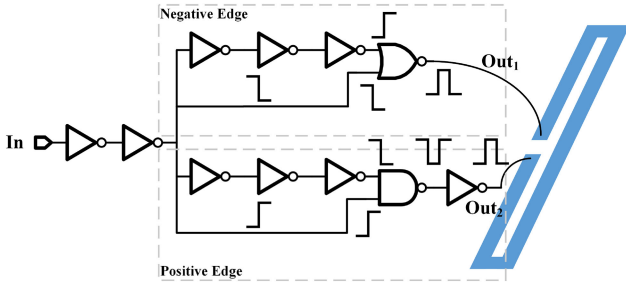


Fig. 1. Circuit schematic of the proposed IR-UWB transmitter.

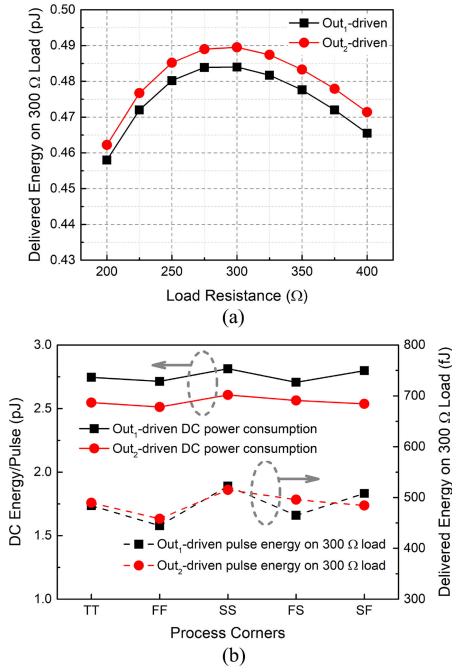


Fig. 2. Pulse generator circuit optimization. (a) The pulse generator is designed to maximize the power transfer efficiency to a 300 Ω load. (b) DC energy per pulse and the delivered impulse energy on 300 Ω load in different process corners.

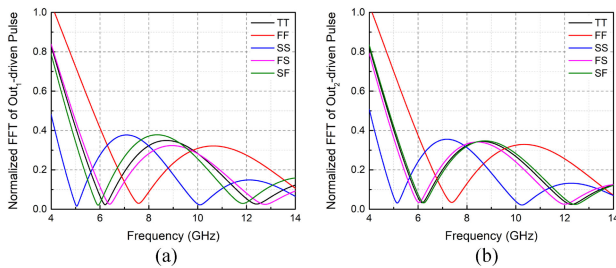


Fig. 3. Normalized FFT of (a) Out_1 -driven and (b) Out_2 -driven pulses on 300 Ω load.

The radiation pattern of the antenna at 8 GHz is shown in Fig. 5(a) with the maximum gain of 3.4 dBi. S_{11} is defined with respect to 300 Ω and plotted in Fig. 5(b). The corresponding matching efficiency, i.e., $1 - \text{mag}(S_{11})^2$, is calculated. -10-dB-bandwidth of the antenna is 7.8–9.5 GHz, effectively acting as a pulse-shaping filter.

4. Measurement results

The photograph of the overall transmitter as implemented

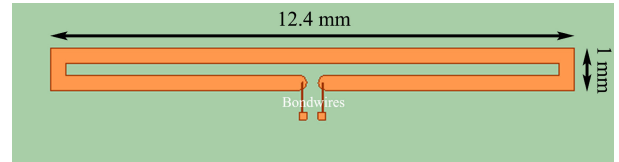


Fig. 4. Planar geometry of the folded-dipole antenna.

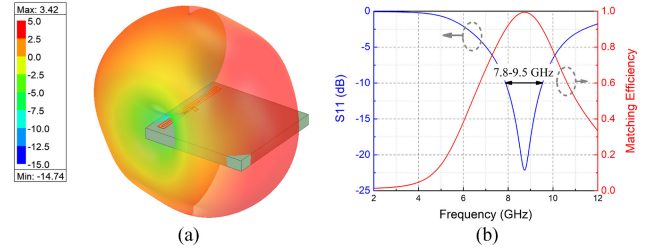


Fig. 5. Antenna performance. (a) Radiation pattern at 8 GHz (unit: dBi). (b) S_{11} and the corresponding matching efficiency with respect to 300 Ω.

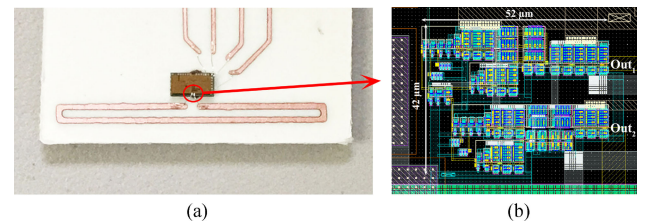


Fig. 6. Transmitter and IC fabrication. (a) Photograph of the IR-UWB transmitter as implemented. (b) Circuit layout of the pulse generator.

is shown in Fig. 6(a). The antenna is fabricated on a Rogers 4350 substrate. The layout of the pulse generator IC, fabricated in TSMC 180-nm CMOS process, only occupies an area of 52 μm × 42 μm as shown in Fig. 6(b).

The transmitter is wirelessly tested with a 6–12 GHz horn antenna (LB-OH-112-10, AINFO Inc.) that features a directivity of 10 dBi. The horn antenna is positioned 20 cm above the transmitter with the same polarization direction as shown in Fig. 7(a). It is followed by a three-stage cascaded LNA (two ZX60-14012L+, one ZX60-153LN-S+, Mini-Circuits, Inc.) with a total gain of 36 dB (including cable loss). The waveforms of Out_1 -driven and Out_2 -driven pulses wirelessly measured with a 25 Gsample/s oscilloscope are shown in Fig. 7(b) and (c), respectively.

With the transmitter operating at 100 Mpulse/s, the Rx power spectrum observed on a spectrum analyzer with a resolution bandwidth of 1 MHz is shown in Fig. 8(a). The effective isotropic radiated power (EIRP) can then be calculated according to the Friis transmission equation,

$$EIRT_{TX} = P_{Rx} - D_{Rx} - 20 \log_{10}(\lambda/4\pi d) \quad (1)$$

where P_{Rx} is the received power density, D_{Rx} is the directivity of the Rx antenna, λ is the frequency-specific wavelength, and d is the Tx-Rx distance. The EIRP is calculated as plotted in Fig. 8(b). The emission limit of UWB protocol is defined in EIRP with the FCC mask shown in the same figure [30]. The experiment demon-

Table I. Performance comparison of edge-combining based IR-UWB transmitters.

	[16]	[14]	[15]	[17]	This work
Technology	65 nm	180 nm	180 nm	130 nm	180 nm
Method	pulse-combining	pulse-combining	filtered edge-combining	filtered edge-combining	antenna co-design
Bandwidth	3.1–8 GHz	6–10 GHz	3.5–6.5 GHz	6.8 GHz	6.8–9 GHz
Pulse Rate	10 M/s	750 M/s	250 M/s	100 M/s	100 M/s
Supply Voltage	1.2 V	1.8–2.2 V	1.8 V	1.2 V	1.5 V
Energy/Pulse	21.6 pJ	12 pJ	86 pJ	38.4 pJ	2.6 pJ
IC Area	0.03 mm ²	0.045 mm ²	0.22 mm ²	0.54 mm ²	0.002 mm²

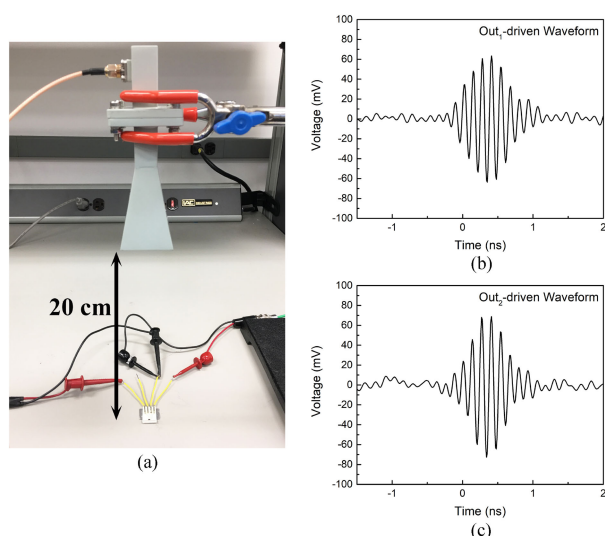


Fig. 7. Measurement setup and the received transient waveforms. (a) Photograph of the benchtop measurement setup. (b) Out_1 -driven pulse waveform. (c) Out_2 -driven pulse waveform.

strates that 100 Mpulse/s operation of the transmitter satisfies the FCC regulation.

A performance comparison with state-of-the-art edge-combining based IR-UWB transmitters is shown in Table I. This work significantly reduces the power consumption with the antenna-and-pulse-generator codesign method and achieves very small IC/overall-device footprints. It does not require any additional passive components either on-chip or off-chip.

5. Conclusion

This work presents a novel concept of antenna-and-pulse-generator codesign to realize FCC-regulation-compliant IR-UWB transmitters for size-restricted and ultra-low-power applications. The transmitter co-optimizes a Gaussian mono-pulse generator and a 300- Ω -input-impedance folded-dipole antenna eliminating any matching or filtering sections. Each impulse emission consumes an average DC energy of 2.6 pJ. Operation at 100 Mpulse/s suffices the FCC regulation limit and shows the -10 -dB-bandwidth to be 6.8–8.6 GHz. The IR-UWB transmitter of this kind shows promise for applications such as miniaturized medical implants.

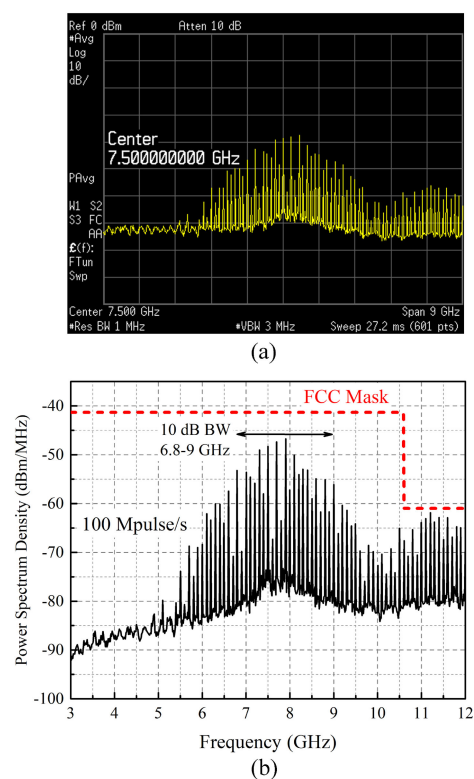


Fig. 8. Power spectral density of the transmitter operating at 100 Mpulse/s. (a) Screenshot of the Rx power spectrum analyzer. (b) Calculated EIRP of the transmitter.

References

- [1] H. Bahrami, *et al.*: “Flexible, polarization-diverse UWB antennas for implantable neural recording systems,” *IEEE Trans. Biomed. Circuits Syst.* **10** (2016) 38 (DOI: [10.1109/TBCAS.2015.2393878](https://doi.org/10.1109/TBCAS.2015.2393878)).
- [2] C. I. Dorta-Quiñones, *et al.*: “A wireless FSCV monitoring IC with analog background subtraction and UWB telemetry,” *IEEE Trans. Biomed. Circuits Syst.* **10** (2016) 289 (DOI: [10.1109/TBCAS.2015.2421513](https://doi.org/10.1109/TBCAS.2015.2421513)).
- [3] S. A. Mirbozorgi, *et al.*: “A single-chip full-duplex high speed transceiver for multi-site stimulating and recording neural implants,” *IEEE Trans. Biomed. Circuits Syst.* **10** (2016) 643 (DOI: [10.1109/TBCAS.2015.2466592](https://doi.org/10.1109/TBCAS.2015.2466592)).
- [4] J. K. Brown, *et al.*: “An ultra-low-power 9.8 GHz crystal-less UWB transceiver with digital baseband integrated in 0.18 μ m BiCMOS,” *ISSCC Dig. Tech. Papers* (2013) 442 (DOI: [10.1109/ISSCC.2013.6487806](https://doi.org/10.1109/ISSCC.2013.6487806)).
- [5] M. S. Chae, *et al.*: “A 128-channel 6 mW wireless neural recording IC with spike feature extraction and UWB transmitter,” *IEEE Trans. Neural Syst. Rehabil. Eng.* **17** (2009) 312 (DOI: [10.1109/](https://doi.org/10.1109/)

TNSRE.2009.2021607).

- [6] H. Ando, *et al.*: “Wireless multichannel neural recording with a 128-Mbps UWB transmitter for an implantable brain-machine interfaces,” *IEEE Trans. Biomed. Circuits Syst.* **10** (2016) 1068 (DOI: [10.1109/TBCAS.2016.2514522](https://doi.org/10.1109/TBCAS.2016.2514522)).
- [7] H. B. Lim, *et al.*: “A human body model for efficient numerical characterization of UWB signal propagation in wireless body area networks,” *IEEE Trans. Biomed. Eng.* **58** (2010) 689 (DOI: [10.1109/TBME.2010.2091128](https://doi.org/10.1109/TBME.2010.2091128)).
- [8] N. Singh, *et al.*: “Design and performance of wearable ultrawide band textile antenna for medical applications,” *Microw. Opt. Technol. Lett.* **57** (2015) 1553 (DOI: [10.1002/mop.29131](https://doi.org/10.1002/mop.29131)).
- [9] K. M. Thotaheva, *et al.*: “SAR, SA, and temperature variation in the human head caused by IR-UWB implants operating at 4 GHz,” *IEEE Trans. Microw. Theory Techn.* **61** (2013) 2161 (DOI: [10.1109/TMTT.2013.2250515](https://doi.org/10.1109/TMTT.2013.2250515)).
- [10] M. R. Yuce, *et al.*: “Wideband communication for implantable and wearable systems,” *IEEE Trans. Microw. Theory Techn.* **57** (2009) 2597 (DOI: [10.1109/TMTT.2009.2029958](https://doi.org/10.1109/TMTT.2009.2029958)).
- [11] K. M. Thotaheva, *et al.*: “Propagation, power absorption, and temperature analysis of UWB wireless capsule endoscopy devices operating in the human body,” *IEEE Trans. Microw. Theory Techn.* **63** (2015) 3823 (DOI: [10.1109/TMTT.2015.2482492](https://doi.org/10.1109/TMTT.2015.2482492)).
- [12] D. Anzai, *et al.*: “Experimental evaluation of implant UWB-IR transmission with living animal for body area networks,” *IEEE Trans. Microw. Theory Techn.* **62** (2013) 183 (DOI: [10.1109/TMTT.2013.2291542](https://doi.org/10.1109/TMTT.2013.2291542)).
- [13] N. Chahat, *et al.*: “A compact UWB antenna for on-body applications,” *IEEE Trans. Antennas Propag.* **59** (2011) 1123 (DOI: [10.1109/TAP.2011.2109361](https://doi.org/10.1109/TAP.2011.2109361)).
- [14] V. V. Kulkarni, *et al.*: “A 750 Mb/s, 12 pJ/b, 6-to-10 GHz CMOS IR-UWB transmitter with embedded on-chip antenna,” *IEEE J. Solid-State Circuits* **44** (2009) 394 (DOI: [10.1109/JSSC.2008.2011034](https://doi.org/10.1109/JSSC.2008.2011034)).
- [15] P. Gunturi, *et al.*: “A 250-mb/s data rate ir-uw b transmitter using current-reused technique,” *IEEE Trans. Microw. Theory Techn.* **65** (2017) 4255 (DOI: [10.1109/TMTT.2017.2695189](https://doi.org/10.1109/TMTT.2017.2695189)).
- [16] Z. Zhang, *et al.*: “A miniature mode reconfigurable inductorless IR-UWB transmitter–receiver for wireless short-range communication and vital-sign sensing,” *IEEE J. Emerg. Sel. Topics Circuits Syst.* **8** (2018) 294 (DOI: [10.1109/JETCAS.2018.2799930](https://doi.org/10.1109/JETCAS.2018.2799930)).
- [17] S. Bourdel, *et al.*: “A 9-pJ/pulse 1.42-V_{pp} OOK CMOS UWB pulse generator for the 3.1–10.6-GHz FCC band,” *IEEE Trans. Microw. Theory Techn.* **58** (2010) 65 (DOI: [10.1109/TMTT.2009.2035959](https://doi.org/10.1109/TMTT.2009.2035959)).
- [18] C. A. Balanis: *Antenna Theory: Analysis and Design* (Wiley, New York, 2016) 4th ed. 506.
- [19] Y. Choi, *et al.*: “Design of modified folded dipole antenna for UHF RFID tag,” *Electron. Lett.* **45** (2009) 387 (DOI: [10.1049/el.2009.0198](https://doi.org/10.1049/el.2009.0198)).
- [20] F.-R. Hsiao and K.-L. Wong: “Omnidirectional planar folded dipole antenna,” *IEEE Trans. Antennas Propag.* **52** (2004) 1898 (DOI: [10.1109/TAP.2004.831337](https://doi.org/10.1109/TAP.2004.831337)).
- [21] H.-Y. Lin, *et al.*: “Performance of implantable folded dipole antenna for in-body wireless communication,” *IEEE Trans. Antennas Propag.* **61** (2013) 1363 (DOI: [10.1109/TAP.2012.2227099](https://doi.org/10.1109/TAP.2012.2227099)).
- [22] B. You, *et al.*: “Dual-frequency folded dipole antenna with PBG structure,” *Electron. Lett.* **45** (2009) 594 (DOI: [10.1049/el.2009.0764](https://doi.org/10.1049/el.2009.0764)).
- [23] S. Tanaka, *et al.*: “Wideband planar folded dipole antenna with self-balanced impedance property,” *IEEE Trans. Antennas Propag.* **56** (2008) 1223 (DOI: [10.1109/TAP.2008.922683](https://doi.org/10.1109/TAP.2008.922683)).
- [24] H. Lyu, *et al.*: “A 430-MHz wirelessly powered implantable pulse generator with intensity/rate control and sub-1 μ A quiescent current consumption,” *IEEE Trans. Biomed. Circuits Syst.* **13** (2019) 180 (DOI: [10.1109/TBCAS.2018.2879357](https://doi.org/10.1109/TBCAS.2018.2879357)).
- [25] H. Lyu, *et al.*: “An energy-efficient wirelessly powered millimeter-scale neurostimulator implant based on systematic codesign of an inductive loop antenna and a custom rectifier,” *IEEE Trans. Biomed. Circuits Syst.* **12** (2018) 1131 (DOI: [10.1109/TBCAS.2018.2852680](https://doi.org/10.1109/TBCAS.2018.2852680)).
- [26] M. M. Ghanbari, *et al.*: “17.5 A 0.8 mm³ ultrasonic implantable wireless neural recording system with linear AM backscattering,” *ISSCC Dig. Tech. Papers* (2019) 284 (DOI: [10.1109/ISSCC.2019.8662295](https://doi.org/10.1109/ISSCC.2019.8662295)).
- [27] D. Seo, *et al.*: “Wireless recording in the peripheral nervous system with ultrasonic neural dust,” *Neuron* **91** (2016) 529 (DOI: [10.1016/j.neuron.2016.06.034](https://doi.org/10.1016/j.neuron.2016.06.034)).
- [28] A. Agarwal, *et al.*: “A wireless, low-drift, implantable intraocular pressure sensor with parylene-on-oil encapsulation,” *CICC Dig. Tech. Papers* (2018) 1 (DOI: [10.1109/CICC.2018.8357049](https://doi.org/10.1109/CICC.2018.8357049)).
- [29] A. Agarwal, *et al.*: “A 4 μ W, ADPLL-based implantable amperometric biosensor in 65 nm CMOS,” *VLSI Dig. Tech. Papers* (2017) 108 (DOI: [10.23919/VLSIC.2017.8008566](https://doi.org/10.23919/VLSIC.2017.8008566)).
- [30] F. C. Commission: “First report and order 02-48,” FCC, February, 2002.